Applied Physics Letters

RESEARCH ARTICLE | MAY 08 2024

Wide-range thermal conductivity modulation based on protonated nickelate perovskite oxides

Special Collection: Advances in Thermal Phonon Engineering and Thermal Management

Hao-Bo Li ; Zhiping Bian ; Mitsuki Yoshimura ; Kohei Shimoyama; Chengchao Zhong ; Keiji Shimoda ; Azusa N. Hattori ; Kunihiko Yamauchi ; Ikutaro Hamada ; Hiromichi Ohta ; Hidekazu Tanaka

Appl. Phys. Lett. 124, 191901 (2024)
https://doi.org/10.1063/5.0201268

Wide-range thermal conductivity modulation based on protonated nickelate perovskite oxides

Cite as: Appl. Phys. Lett. **124**, 191901 (2024); doi: 10.1063/5.0201268
Submitted: 30 January 2024 · Accepted: 14 April 2024 ·
Published Online: 8 May 2024

Hao-Bo Li,[1,2,a)] Zhiping Bian,[3] Mitsuki Yoshimura,[3] Kohei Shimoyama,[1] Chengchao Zhong,[4] Keiji Shimoda,[4] Azusa N. Hattori,[1,2] Kunihiko Yamauchi,[5] Ikutaro Hamada,[6] Hiromichi Ohta,[7,a)] and Hidekazu Tanaka[1,2,a)]

AFFILIATIONS

[1]SANKEN, Osaka University, Ibaraki, Osaka 567-0047, Japan
[2]Spintronics Research Network Division, Institute for Open and Transdisciplinary Research Initiatives, Osaka University, Yamadaoka 2-1, Suita, Osaka 565-0871, Japan
[3]Graduate School of Information Science and Technology, Hokkaido University, Sapporo 060-0814, Japan
[4]Department of Applied Chemistry, Graduate School of Life Sciences, Ritsumeikan University, 1-1-1 Nojihigashi, Kusatsu, Shiga 525-8577, Japan
[5]Center for Spintronics Research Network, Osaka University, Toyonaka, Osaka 560-8531, Japan
[6]Department of Precision Engineering, Graduate School of Engineering, Osaka University, Suita, Osaka 565-0871, Japan
[7]Research Institute for Electronic Science, Hokkaido University, Sapporo 001-0020, Japan

Note: This paper is part of the APL Special Collection on Advances in Thermal Phonon Engineering and Thermal Management.
[a)]**Authors to whom correspondence should be addressed:** h.b.li.phys@sanken.osaka-u.ac.jp; hiromichi.ohta@es.hokudai.ac.jp; and h-tanaka@sanken.osaka-u.ac.jp

ABSTRACT

The perovskite oxides $ReNiO_3$ (Re = rare-earth elements) are promising functional materials due to their strongly correlated electrons. Except for the well-known intrinsic metal-insulating transition in these materials, recent progresses have proved that protonation of $ReNiO_3$ can bring about interesting Mott transition in this series. To date, in these protonated species (H-$ReNiO_3$), huge resistance switching, fast ionic diffusion, and their applications as an iontronic transistor, memristor, and fuel cell are reported. In this work, the thermal conductivities of H-$ReNiO_3$ (Re = La, Nd, Sm, and Eu) epitaxial thin films are investigated. The protonation-induced Mott transition can effectively modulate the electronic thermal conductivity while the lattice thermal conductance is less affected. Hence, at room temperature, the metallic $LaNiO_3$ and $NdNiO_3$ exhibit reversible wide thermal conductivity modulation, in ranges of 2.6–12.0 and 1.6–8.0 $W\,m^{-1}\,K^{-1}$, respectively. These values are much larger than other thermal regulation materials based on transition metal oxides. Thus, our work reveals the great potential of $ReNiO_3$ being applied as a thermal-regulating material. The fast ionic diffusion in H-$ReNiO_3$ also guarantees that a fast response and wide-range thermal transistor can be realized by H-$LaNiO_3$ and H-$NdNiO_3$ in the future.

Strongly correlated materials are known to exhibit characteristic properties, such as high-temperature superconductivity, multiferroics, etc., due to the strong interactions between different degrees of freedom.[1] Among the strongly correlated oxides, transition metal perovskite $ReNiO_3$ (Re = rare-earth elements) have been investigated for decades as representative charge-transfer insulators with an intrinsic metal–insulator transition (MIT).[2] In particular, the induced near-room temperature MIT (e.g., $NdNiO_3$ ~200 K; $SmNiO_3$ ~400 K) can lead to potential applications such as Mott transistors, which may benefit the realization of beyond CMOS devices.[3] In recent years, another type of metal–insulator transition has been observed in $SmNiO_3$ (SNO) and $NdNiO_3$ (NNO) after protonation. Unlike the conventional mechanism, the proton injection-induced MIT is resulted from the B-site reduction (Ni^{3+} to Ni^{2+}), which subsequently increases the Coulomb repulsion between electrons in the e_g orbital.[4]

Recently, researchers have found that an external electric field can simultaneously control the proton diffusion and induce the huge resistance change in $SmNiO_3$ up to 10^8.[5] The high insulating property and high proton diffusion speed allow the protonated $ReNiO_3$ (H-$ReNiO_3$) to be applied as an electrolyte in solid state fuel cells

(SOFCs).[6] More importantly, the diffusion of proton in H-$ReNiO_3$ can be controlled by an external electric field. This suggests protonated $ReNiO_3$ materials (H-$ReNiO_3$) are promising candidates in future iontronic devices and inspires various designs, such as proton memristors, artificial synapses, and proton sensors.[4,7,8] Although these achievements indicate the large potential of H-$ReNiO_3$ being applied in various circumstances, current research primarily focuses on tuning electronic and ionic conductivities. Other controllable parameters, such as thermal conductivity, is far less investigated. Hence, further exploration of controllable and switchable properties (e.g., thermal conductivity) in protonated $ReNiO_3$ materials is highly in need.

In this work, we fabricated epitaxial thin films of $ReNiO_3$ (Re = La, Nd, Sm, and Eu) on $La_{0.18}Sr_{0.82}Al_{0.59}Ta_{0.41}O_3$ (LSAT). A reversible thermal conductivity modulation controlled by protonation and deprotonation is investigated. Among the four species, the $LaNiO_3$ and $NdNiO_3$ exhibit surprisingly wide-range thermal conductivity modulations of 2.6–12.0 $W\,m^{-1}\,K^{-1}$ (H-$LaNiO_3$ and $LaNiO_3$) and 1.6–8.0 $W\,m^{-1}\,K^{-1}$ (H-$NdNiO_3$ and $NdNiO_3$), respectively. Especially for the $LaNiO_3$ case, the room temperature thermal regulation range is much wider than previously reported thermal conductivity control in transition metal oxides, such as $SrCoO_{2.5}$, $La_{0.5}Sr_{0.5}CoO_{3-\delta}$, and WO_3.[9–12] The thermal conductivity modulation is mainly a result of greatly suppressed electronic thermal conductivity (κ_{ele}) after protonation, which is closely related to the proton-induced metal–insulator transition in $LaNiO_3$ and $NdNiO_3$. For the insulating $SmNiO_3$ and $EuNiO_3$, it is found that the lattice thermal conductivity is hardly affected (κ_{lat}) after protonation, which might be attributed to the small mass of proton and unchanged unit cell shape after protonation. Our work reports not only the thermal conductivities of one series of functional materials but also reveals the potential of these materials being applied to thermal regulation applications.

The $ReNiO_3$ (Re = La, Nd, Sm, and Eu) thin films were fabricated on [100]-oriented single crystal $La_{0.18}Sr_{0.82}Al_{0.59}Ta_{0.41}O_3$ (LSAT) substrate (cubic, $a = 3.868$ Å) by pulsed laser deposition (PLD). The thin films were synthesized with temperature ranging from 620 to 650 °C, with oxygen pressure from 30 to 50 Pa. The ArF excimer laser (193 nm) at 4 Hz and 90 mJ were adopted. The crystal structure and crystalline quality of the thin film were characterized by x-ray diffraction (XRD, SmartLab, Rigaku). For protonation, the electrochemical protonation using ionic liquid gating was adopted,[13] and the demonstration of the sample setup is shown in supplementary material Fig. S1. The gating electrode was composed of a Pt coil. The bottom electrode connecting the ground was made of conductive silver adhesive (SPI, 04999-AB) painted around the sample surface. After electrode preparation, the sample was soaked in an ionic liquid of N,N-Diethyl-N-methyl-N-(2-methoxyethyl)ammonium bis(trifluoromethanesulfonyl)imide (DEME-TFSI). With a gating voltage of +3.5 V for 60 min at room temperature, the $ReNiO_3$ thin film was protonated, and the estimated proton ratio was 1.0 per $ReNiO_3$ formula unit cell. For H-$LaNiO_3$, H-$SmNiO_3$, and H-$NdNiO_3$, the proton ratio was deduced from the relationship between resistance change and proton concentration measured by nuclear reaction analysis.[14] For H-$EuNiO_3$, x-ray photoelectron spectroscopy (XPS) of Ni $2p_{3/2}$ was adopted to estimate the proton ratio indirectly (supplementary material Fig. S2). The conductivities of thin films were measured by a physical property measurement system (PPMS, Quantum design). The thermal conductivity (κ) of the $ReNiO_3$ and H_xReNiO_3 films perpendicular to the substrate surface was measured by TDTR (PicoTR, PicoTherm). With a picosecond thermoreflectance analyzer, PicoTR, laser pulses (pump laser) of 0.5 ps pulse width are applied to the sample with a time period of 50 ns. The temperature response is detected with the probe laser. The top side of the Pt film was deposited as the transducer. The decay curves of the TDTR phase signals were simulated to obtain κ by integrated software. In order to calculate the thermal conductivity of the thin film, the lattice thermal conductivity from a blank LSAT substrate was collected as well. The first-principle calculations are adopted to obtain the crystal structures of H-$ReNiO_3$, and the details are declared in supplementary material.

Protonation of $ReNiO_3$ is achieved by ionic liquid gating at room temperature as shown in Fig. 1. The water molecules are decomposed at the thin film surface and protons diffuse into $ReNiO_3$ due to a chemical potential difference.[13] Deprotonation can be realized by two approaches: (1) ionic liquid gating with reversed voltage and (2) annealing the H-$ReNiO_3$ in the air at 400 °C. Deprotonated samples can be protonated again by ionic liquid gating, allowing reversible control between $ReNiO_3$ and H-$ReNiO_3$. Crystal structures before and after protonation were measured by out-of-plane x-ray diffraction. As shown in Figs. 2(a) and 2(d), the pseudo-cubic $(00l)_{pc}$ peak of $ReNiO_3$ can be identified, indicating that the $ReNiO_3$ thin film is *c*-axis oriented on the LSAT substrate. The out-of-plane pseudo-cubic lattice constants of the as-grown $ReNiO_3$ (Re = La, Nd, Sm, and Eu) thin films are 3.814, 3.801, 3.814, and 3.818 Å, respectively, as summarized in Fig. 2(e), in excellent agreements with previous reports.[15–18] Protonation leads to a lattice expansion along the *c*-axis in all samples, where the c_{pc} of H-$ReNiO_3$ (Re = La, Nd, Sm, and Eu) are 3.982, 4.145, 4.059, and 3.945 Å, respectively, consistent with previous reports.[4,7,19] A different observed expansion ratio might be related to the different tilting angle of the NiO_6 octahedron due to strain effects. The residual peaks of the as-grown state contribute to the area beneath the electrode, which would not influence the measurement of thermal conductivity and resistivity (supplementary material Fig. S1). By heating the sample in the air as mentioned in Fig. 1, deprotonation is achieved, and the lattice parameters c_{pc} of the deprotonated samples are slightly larger than the as-grown samples which might be related to the creation of oxygen vacancy after heating.[7] This allows repeatedly controlling thermal conductivity, which will be discussed later, by switching phases between $ReNiO_3$ and H-$ReNiO_3$.

Next, the room temperature thermal conductivity (κ) of $ReNiO_3$, H-$ReNiO_3$, and deprotonated $ReNiO_3$ series are evaluated at room temperature by time domain thermos reflectance (TDTR), which is known as an effective approach to obtain the thermal conductivity of a thin film.[10,19–27] In order to extract the thermal conductivity, the densities of the $ReNiO_3$ series are referred to as experimental values and those of H-$ReNiO_3$ are calculated from the crystal structure obtained by calculations based on the density functional theory with the on-site Coulomb interaction (DFT+*U*) (supplementary material Figs. S3 and S4 and Ref. 28). As described in the inset of Fig. 3(a), based on the parameters demonstrated in supplementary material Table S1, the total thermal conductivity (κ) of as-grown $ReNiO_3$ (Re = La, Nd, Sm, and Eu) thin films are estimated to be 11.6, 8.0, 1.8, and 2.5 $W\,m^{-1}\,K^{-1}$, respectively, [Figs. 3(a) and 3(d)]. After performing protonation, the measured curves of $LaNiO_3$ and $NdNiO_3$ exhibit a clear difference from the as-grown state: the thermal conductivities are greatly suppressed to 2.6 $W\ m^{-1}\ K^{-1}$ for H-$LaNiO_3$ and 1.6 $W\ m^{-1}\ K^{-1}$ for H-$NdNiO_3$.

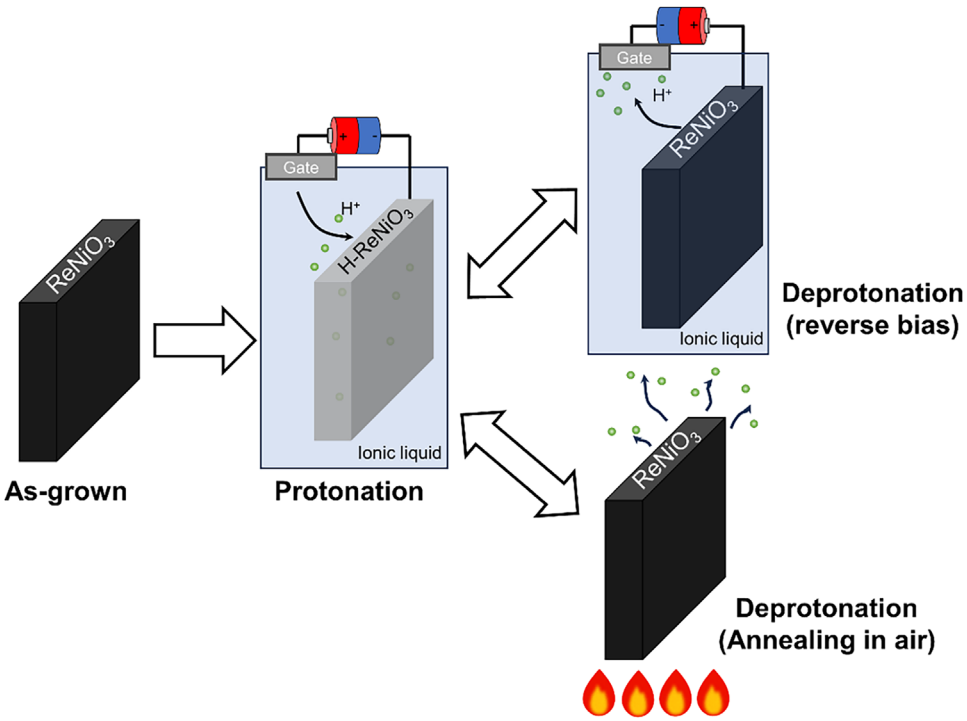

FIG. 1. The protonation by ionic liquid gating and two reversible approaches to realize deprotonation.

However, for insulating $SmNiO_3$ and $EuNiO_3$, although the TDTR curves confirm the reversibility, the protonation-induced thermal conductivity change is much smaller than that in $LaNiO_3$ and $NdNiO_3$, where κ changes from 1.8 to 1.6 $W\,m^{-1}\,K^{-1}$ for $SmNiO_3$ and from 2.5 to 3.0 $W\,m^{-1}\,K^{-1}$ for $EuNiO_3$. Interestingly, the thermal conductivity slight increases in $EuNiO_3$ after protonation. In addition, the κ of the as-grown status is recovered after deprotonation [Fig. 3(e)]. This observation, together with the diffraction evidence showing the structural

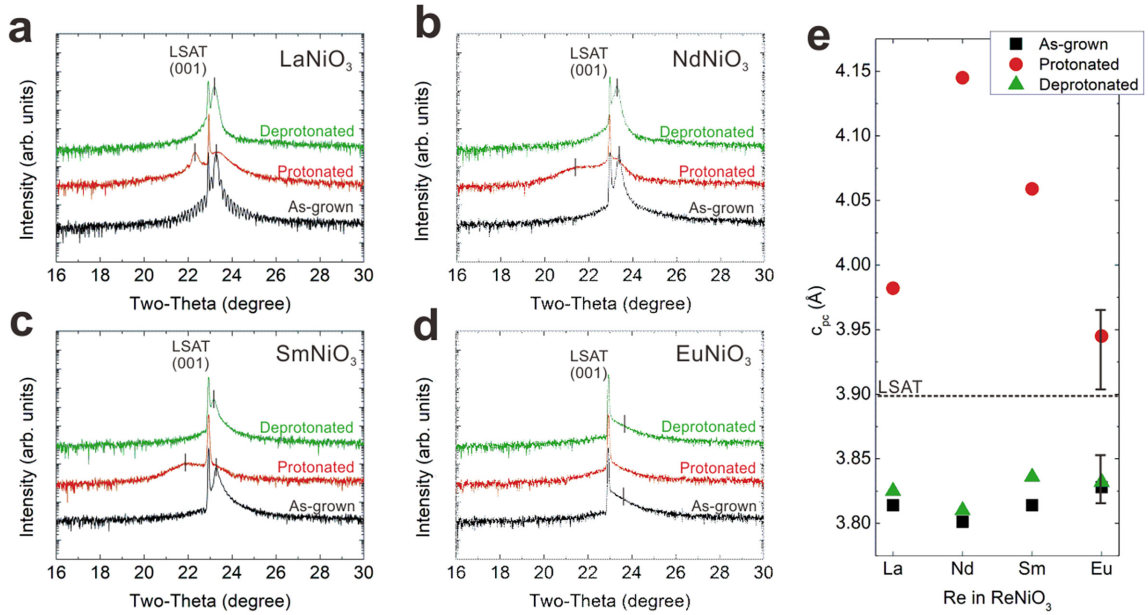

FIG. 2. (a)–(d) Out-of-plane XRD of $ReNiO_3$ (Re = La, Sm, Nd, and Eu) $(001)_{pc}$ peak before and after protonation. Since the top electrode is covering the part of the sample surface, protonation is difficult to proceed in that area. Hence, a residual peak can be observed in the XRD of the protonated samples. The structural reproducibility is examined by performing deprotonation annealing in the air. (e) Summarization of out-of-plane lattice expansion. The error of $EuNiO_3$ could be large due to the weak intensity of the XRD peak.

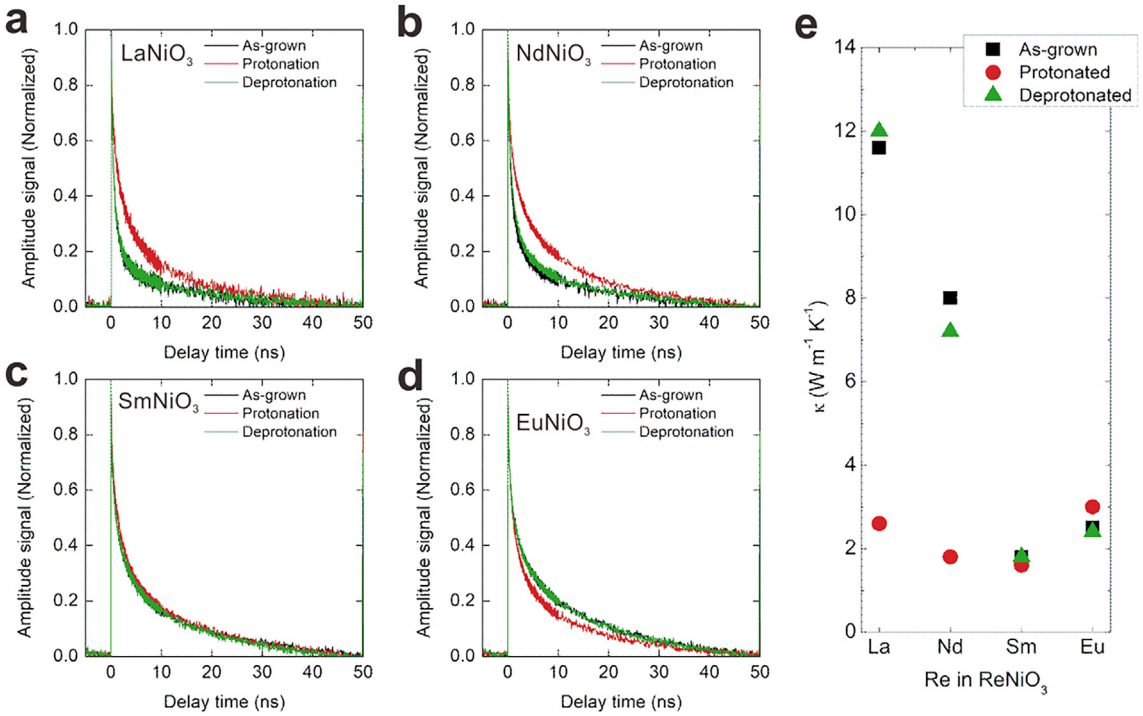

FIG. 3. (a)–(d) Original TDTR decay curves of as-grown, protonated, and deprotonated $ReNiO_3$ (Re = La, Sm, Nd, and Eu) measured at room-temperature. The original data of each material are demonstrated in (a)–(d). (e) is a summary of the thermal conductivity modulation of $ReNiO_3$ before and after protonation and the reproducibility is verified. Among all, $LaNiO_3$ and $NdNiO_3$ exhibit a wide-range modulation of thermal conductivity.

recovery in Fig. 2, suggests that the wide-range thermal regulation in $LaNiO_3$ and $NdNiO_3$ is fully reversible by protonation and deprotonation.

Figure 4(a) summarizes the relationship between thermal conductivity (κ) and electrical conductivity of $ReNiO_3$ and H-$ReNiO_3$. In the pristine states of $LaNiO_3$ and $NdNiO_3$, the total thermal conductivity (κ) could be mainly governed by electronic thermal conductivity (κ_{ele}) due to their metallic nature at room temperature. It is assumed that κ of $LaNiO_3$ and $NdNiO_3$ could be roughly estimated by the Wiedemann–Franz law: $\kappa/\sigma = LT$, where σ, T, and L are electronic conductivity, temperature, and Lorenz number, respectively. As shown in Fig. 4(a), the measured data have a good agreement with the model while the fitted

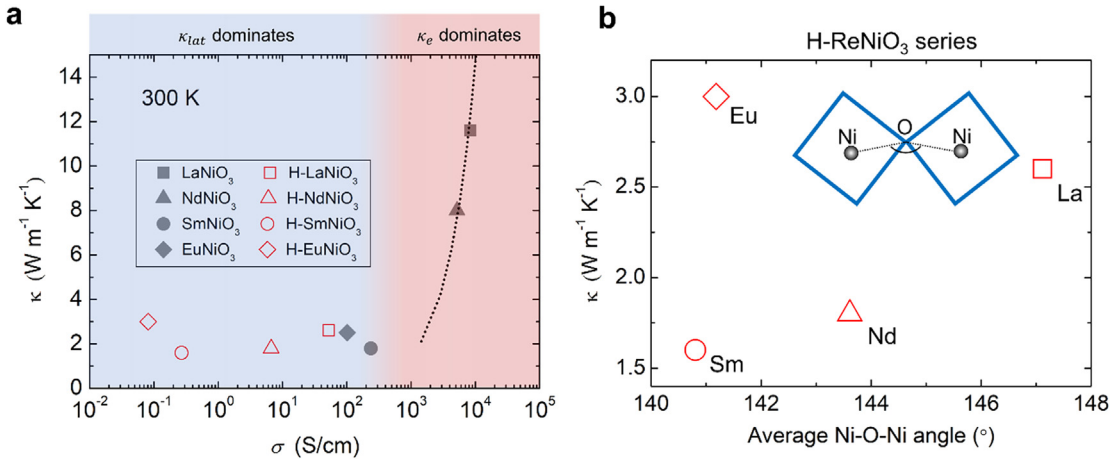

FIG. 4. (a) Thermal conductivity (κ) vs electrical conductivity (σ) of $ReNiO_3$ and H-$ReNiO_3$ series. The dotted line indicates the Wiedemann–Franz law with Lorentz number of 4.89×10^{-8} $W\Omega K^{-2}$. (b) Thermal conductivity (κ) vs Ni–O–Ni bond angle of H-$ReNiO_3$. The bond angle is summarized from DFT calculated crystal structure as demonstrated in supplementary material Fig S4. Aside from H-$EuNiO_3$, the thermal conductivity increases along with the increasing Ni–O–Ni angle.

Lorenz number (L) for $LaNiO_3$ and $NdNiO_3$ could be larger than the classical value. It might be related to the strong correlation of the electron in these systems,[29] and this would be investigated in our future work. Oppositely, $SmNiO_3$ and $EuNiO_3$ are insulating at room-temperature; we assume that in these two species, the lattice thermal conductivity (κ_{lat}) is dominant. The small electrical conductivity of $\sim 2.4 \times 10^2$ S/cm ($SmNiO_3$) and $\sim 1.0 \times 10^2$ S/cm ($EuNiO_3$) implies that the κ_{ele} in $SmNiO_3$ and $EuNiO_3$ could be negligible.

After protonation, Ni^{3+} is reduced to Ni^{2+}, and the electrons become localized due to strong Coulomb repulsion between two e_g electrons in Ni^{2+}. Thus, the dominating κ_{ele} in $LaNiO_3$ and $NdNiO_3$ are greatly suppressed in H-$LaNiO_3$ and H-$NdNiO_3$, and the electrical conductivity decreases by $\sim$3 orders of magnitude. Therefore, the intrinsic κ_{lat} becomes dominant in the protonated samples instead, leading to a wide-range modulation of thermal conductivity. We noted that changing oxygen content can also bring about a metal–insulator transition in perovskite oxides, typically leading to an electrical conductivity modulation of $\sim 10^5$ (e.g., $La_{0.5}Sr_{0.5}CoO_{2.5} \leftrightarrow La_{0.5}Sr_{0.5}CoO_{3-\delta}$, and $SrCoO_{2.5} \leftrightarrow SrCoO_3$). However the accompanied thermal conductivity modulation between $SrCoO_{2.5}$ and $SrCoO_3$ is in the range of 1.70–4.33 and 0.85–4.6 $W\,m^{-1}\,K^{-1}$ for $La_{0.5}Sr_{0.5}CoO_{3-\delta}$, all narrower than the protonation and deprotonation of $LaNiO_3$ and $NdNiO_3$. However, for $SmNiO_3$ and $EuNiO_3$, where κ_{lat} is dominating in the pristine state, the thermal conductivities are not tuned widely after protonation since electrons are always localized due to strong correlation. Even though the electrical conductivity similarly decreases by $\sim$3 orders of magnitude in $SmNiO_3$ and $EuNiO_3$, protonation hardly changes thermal conductivity. This also implies that the protonation is unable to bring about as much influence on κ_{lat} as κ_{ele} in these compounds, which might be related to the small mass of proton.

Additional insights can be obtained from crystal structural evolution. $SmNiO_3$ and $EuNiO_3$ remain orthorhombic during the protonation process. For all the H-$ReNiO_3$ materials, the thermal conductivity is mainly governed by κ_{lat}; thus, the larger the distortion in the ABO_3 lattice, the lower the thermal conductivity can be anticipated. In order to evaluate the lattice distortion in the H-$ReNiO_3$ series, the average Ni–O–Ni bond angles based on our DFT+U calculations are summarized (supplementary material Table S2, supplementary material Figs. S5 and S6). Figure 4(b) shows that the thermal conductivity decreases along with the decreasing Ni–O–Ni bond angle except for $EuNiO_3$. This indicates that an increment in distortion in the ABO_3 unit cell results in suppressed thermal conductivity as anticipated, where lattice thermal conductivity is highly dependent on the crystal symmetry. H-$EuNiO_3$ could be a special case, in which other parameters, such as magnetism of Eu, might play a role.[30] In $EuNiO_3$, the Eu^{3+} ($J = 0$) ion that should not carry any magnetic moment is reported to be carrying 3.4 μ_B, which is unexpected.[31] Recently, researchers have also found that in the reduced compound $EuVO_2H$, the magnetic ordering between Eu^{2+} can be established by interlayer charge transfer.[32] These reports indicate Eu-based perovskite oxides might be a complicated case and the magnetic ordering of Eu cannot be ignored when analyzing κ_{lat}.

The above results suggest that the protonation suppresses the κ_{ele} greatly instead of κ_{lat}, which is accompanied by Mott transition. As shown in Fig. 5(a), by comparing with other reported materials that are potentially applicable in thermal control,[9–11,33–36] $LaNiO_3$ and $NdNiO_3$ exhibit a wide-range modulation among transition oxides with high upper limits due to their intrinsic metallic nature and crystal symmetry. For instance, metallic $SrCoO_3$ possesses the same cubic structure and close electrical conductivity as that of $LaNiO_3$,; however, the thermal conductivity of $LaNiO_3$ is much higher. More importantly, our result may also imply that the Mott transition in $ReNiO_3$ governed by protonation can be a powerful tool to realize effective thermal control in a material where κ_{ele} can be fully suppressed, i.e., switching between κ_{ele} and κ_{lat} [Fig. 5(b)]. Meanwhile, it is worth noting that the wide-range modulation in $LaNiO_3$ could be also associated with structural switching to some extent, because the proton-induced octahedron tilting in $LaNiO_3$ drives a tetragonal-to-orthorhombic transition, resulting in a more complicated phonon band and reduction of the lattice thermal conductivity. These guarantee that the lower minimum of thermal conductivities (OFF state) is also comparable with other materials, which eventually proves that these materials could be excellent candidates as thermal transistors. Based on above results, we propose a simple guideline, metallic materials with intrinsically high κ_{ele} are suitable precursors to offer a higher upper limit. Then, once the Mott

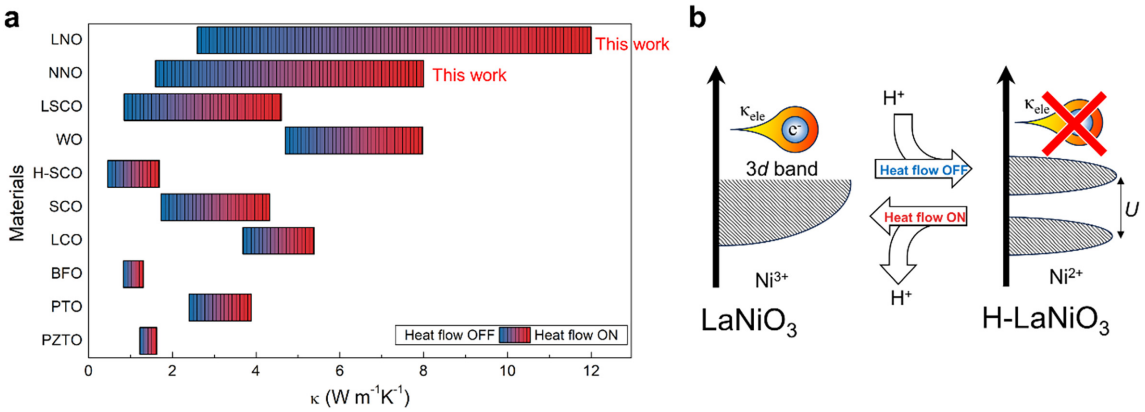

FIG. 5. (a) Thermal conductivity modulation of reported oxide materials and the data are extracted from previous reported oxide materials: $La_{0.5}Sr_{0.5}CoO_{3-\delta}$ (LSCO, Ref. 12), WO_3 (WO, Ref. 13), $SrCoO_{2.5}$ (SCO, Ref. 10, 11), $HSrCoO_{2.5}$ (Ref. 10), Li_xCoO_2 (LCO, Ref. 34), $BiFeO_3$ (BFO, Ref. 35), $PbTiO_3$ (PTO, Ref. 36), and $PbZr_{0.3}Ti_{0.7}O_3$ (PZTO, Ref. 37). (b) The proposed mechanism of a wide-range thermal modulation in $LaNiO_3$ via protonation and deprotonation.

transition can be achieved by protonation in the target material, a wide-range thermal conductivity control could be anticipated. Since the intrinsic κ_{lat} of a material determines the lower limit, a heavier transition metal or rare-earth elements are preferred. Second, to further expand the lower limit of the thermal conductivity, one may consider using heavier elements, such as Li^+ and K^+, instead of protons, since they can also be electrochemically injected into transition metal oxides, such as $Fe_3O_4 + 2Li^+ + 2e^- \rightarrow Li_2(Fe_3O_4)$.[37] This may bring about an additional suppression on κ_{lat} and eventually further enlarge the range of thermal regulation.

In summary, the thermal conductivity of $ReNiO_3$ (Re = La, Nd, Sm, and Eu) thin films grown on LSAT(001) and the protonated phase H-$ReNiO_3$ have been investigated. It is found that the protonation-induced Mott transition can greatly suppress the electronic thermal conductivity and, hence, the metallic $NdNiO_3$ and $LaNiO_3$ exhibit a wide-range thermal modulation range compared with previously reported transition metal oxides. However, the protonation exhibits weak influence on the insulating phases, such as $SmNiO_3$ and $EuNiO_3$, and all H-$ReNiO_3$ (Re = La, Nd, Sm, and Eu) are in the comparable range (all about 2–3 $W\,m^{-1}\,K^{-1}$). Thus, we conclude that the effect of protonation on thermal conductivity in transition metal oxides mainly involves electron-contributed thermal conductivity, while the lattice thermal conductivity is barely affected. Moreover, the deprotonation can be also controlled by electrochemical gating (supplementary material Fig. S7). This further verifies that $NdNiO_3$ and $LaNiO_3$ possess great application potential when applied as thermal transistors or other thermal management devices. Especially, since the fast proton diffusion in $ReNiO_3$ has been proven,[6] wide-range thermal control and fast response speed can be anticipated in $NdNiO_3$- and $LaNiO_3$-based iontronic devices.

See the supplementary material for information about the ionic liquid gating setup, XPS data of H-$EuNiO_3$, TDTR fitting parameters, DFT calculation methods, determination of the crystal structure of H-$ReNiO_3$, Ni–O–Ni bond angle, and reversible thermal modulation via ionic liquid gating.

This study was financially supported by JSPS KAKENHI: Grant-in-Aid for Scientific Research on Innovative Areas "Hydrogenomics" (Nos. JP19H05055 and JP18H05519), JSPS KAKENHI Grant-in-Aid for Young Scientists (22K14475), Grants-in-Aid for Scientific Research A (22H00253) and Innovative Areas (19H05791), Grant-in-Aid for Challenging Research Exploratory (22K18757) from the Japan Society for Promotion of Science (JSPS), and Grant-in-Aid for Scientific Research (B) (23H02045). This work was also partly supported by the Advanced Research Infrastructure for Materials and Nanotechnology Open Facilities in Osaka University, supported by ARIM of MEXT (JPMXP1223NR0016), Cooperative Research Program of Crossover Alliance to Create the Future with People, Intelligence and Materials, Young-scientist FS (2022Y005) and JST SPRING, (JPMJSP2119). The calculations were performed using the facility of the supercomputer center at the Institute for Solid State Physics, the University of Tokyo (DFT). We also thank the members of the Comprehensive Analysis Center, SANKEN, Osaka University, for x-ray diffraction measurements. We thank Dr. Zhu Tong from Kyoto University for advice on English grammar and expressions.

AUTHOR DECLARATIONS

Conflict of Interest

The authors have no conflicts to disclose.

Author Contributions

Hao-Bo Li: Conceptualization (equal); Data curation (lead); Formal analysis (equal); Funding acquisition (equal); Investigation (lead); Methodology (equal); Project administration (supporting); Writing – original draft (lead). **Zhiping Bian:** Data curation (supporting); Software (supporting); Writing – review & editing (supporting). **Mitsuki Yoshimura:** Data curation (supporting); Software (supporting). **Kohei Shimoyama:** Data curation (supporting). **Chengchao Zhong:** Data curation (supporting). **Keiji Shimoda:** Data curation (supporting). **Azusa N. Hattori:** Funding acquisition (supporting); Resources (supporting); Writing – review & editing (supporting). **Kunihiko Yamauchi:** Data curation (supporting); Resources (supporting); Software (supporting); Writing – review & editing (supporting). **Ikutaro Hamada:** Data curation (supporting); Resources (supporting); Software (supporting); Writing – review & editing (equal). **Hiromichi Ohta:** Conceptualization (equal); Funding acquisition (equal); Investigation (equal); Methodology (equal); Project administration (equal); Supervision (equal); Validation (equal); Writing – review & editing (equal). **Hidekazu Tanaka:** Conceptualization (equal); Funding acquisition (equal); Investigation (equal); Methodology (equal); Project administration (equal); Supervision (equal); Validation (equal); Writing – review & editing (equal).

DATA AVAILABILITY

The data that support the findings of this study are available from the corresponding authors upon reasonable request.

REFERENCES

[1]E. Morosan, D. Natelson, A. H. Nevidomskyy, and Q. Si, Adv. Mater. **24**, 4896–4923 (2012).
[2]J. B. Torrance, P. Lacorre, A. I. Nazzal, E. J. Ansaldo, and Ch. Niedermayer, Phys. Rev. B **45**, 8209–8212 (1992).
[3]S. Das, A. Chen, and M. Marinella, "Beyond CMOS," 2021 *IEEE International Roadmap for Devices and Systems Outbriefs, Santa Clara, CA, USA* (IEEE, 2021), pp. 1–129.
[4]Z. Zhang, D. Schwanz, B. Narayanan, M. Kotiuga, J. A. Dura, M. Cherukara, H. Zhou, J. W. Freeland, J. Li, R. Sutarto, F. He, C. Wu, J. Zhu, Y. Sun, K. Ramadoss, S. S. Nonnenmann, N. Yu, R. Comin, K. M. Rabe, S. K. R. S. Sankaranarayanan, and S. Ramanathan, Nature **553**, 68–72 (2018).
[5]J. Shi, Y. Zhou, and S. Ramanathan, Nat. Commun. **5**, 4860 (2014).
[6]Y. Zhou, X. Guan, H. Zhou, K. Ramadoss, S. Adam, H. Liu, S. Lee, J. Shi, M. Tsuchiya, D. D. Fong, and S. Ramanathan, Nature **534**, 231–234 (2016).
[7]Y. Taniguchi, H.-B. Li, K. Shimoyama, A. N. Hattori, and H. Tanaka, Appl. Phys. Lett. **122**, 263502 (2023).
[8]K. Ramadoss, F. Zuo, Y. Sun, Z. Zhang, J. Lin, U. Bhaskar, S. Shin, M. A. Alam, S. Guha, D. Weinstein, and S. Ramanathan, IEEE Electron Device Lett. **39**, 1500–1503 (2018).
[9]Q. Lu, S. Huberman, H. Zhang, Q. Song, J. Wang, G. Vardar, A. Hunt, I. Waluyo, G. Chen, and B. Yildiz, Nat. Mater. **19**, 655–662 (2020).
[10]Q. Yang, H. J. Cho, Z. Bian, M. Yoshimura, J. Lee, H. Jeen, J. Lin, J. Wei, B. Feng, Y. Ikuhara, and H. Ohta, Adv. Func. Mater. **33**, 2214939 (2023).
[11]Y. Zhang, W. M. Postiglione, R. Xie, C. Zhang, H. Zhou, V. Chaturvedi, K. Heltemes, H. Zhou, T. Feng, C. Leighton, and X. Wang, Nat. Commun. **14**, 2626 (2023).

[12]S. Ning, S. C. Huberman, Z. Ding, H.-H. Nahm, Y.-H. Kim, H.-S. Kim, G. Chen, and C. A. Ross, Adv. Mater. **31**, 1903738 (2019).
[13]N. Lu, P. Zhang, Q. Zhang, R. Qiao, Q. He, H.-B. Li, Y. Wang, J. Guo, D. Zhang, Z. Duan, Z. Li, M. Wang, S. Yang, M. Yan, E. Arenholz, S. Zhou, W. Yang, L. Gu, C.-W. Nan, J. Wu, Y. Tokura, and P. Yu, Nature **546**, 124–128 (2017).
[14]I. Matsuzawa, T. Ozawa, Y. Nishiya, U. Sidik, A. N. Hattori, H. Tanaka, and K. Fukutani, Phys. Rev. Mater. **7**, 085003 (2023).
[15]D. Kan, T. Hatano, A. Abe, H. Ikuta, and Y. Shimakawa, Appl. Phys. Lett. **117**, 231602 (2020).
[16]S. Heo, C. Oh, J. Son, and H. M. Jang, Sci. Rep. **7**, 4681 (2017).
[17]S. Catalano, M. Giber, V. Bisogni, O. E. Peil, F. He, R. Sutarto, M. Viret, P. Zubko, R. Scherwitzl, A. Georges, G. A. Sawatzky, T. Schmitt, and J.-M. Triscone, APL Mater. **2**, 116110 (2014).
[18]D. Meyers, S. Middey, M. Kareev, M. van Veenendaal, E. J. Moon, B. A. Gray, J. Liu, J. W. Freeland, and J. Chakhalian, Phys. Rev. B **88**, 075116 (2013).
[19]H. J. Cho, G. Kim, T. Onozato, H. Jeen, and H. Ohta, Int. J. Heat Mass Transfer **137**, 263–267 (2019).
[20]H. J. Cho, B. Feng, T. Onozato, M. Wei, A. V. Sanchela, Y. Ikuhara, and H. Ohta, Phys. Rev. Mater. **3**, 094601 (2019).
[21]Y. Takashima, Y.-Q. Zhang, J. Wei, B. Feng, Y. Ikuhara, H. J. Cho, and H. Ohta, J. Mater. Chem. A **9**, 274–280 (2021).
[22]F. Krahl, Y. Wu, H. J. Cho, M. Karppinen, and H. Ohta, Adv. Electron. Mater. **6**, 2000404 (2020).
[23]G. Kim, B. Feng, Y.-M. Sheu, H. J. Cho, Y. Ikuhara, and H. Ohta, ACS Appl. Electron. Mater. **2**, 2507–2513 (2020).
[24]H. J. Cho, Y. Wu, Y.-Q. Zhang, B. Feng, M. Mikami, W. Shin, Y. Ikuhara, Y.-M. Sheu, K. Saito, and H. Ohta, Adv. Mater. Interfaces **8**, 2001932 (2021).
[25]X. Zhang, Y. Zhang, L. Wu, A. Tsuruta, M. Mikami, H. J. Cho, and H. Ohta, ACS Appl. Mater. Interfaces **14**, 33355–33360 (2022).
[26]Z. Bian, Q. Yang, M. Yoshimura, H. J. Cho, J. Lee, H. Jeen, T. Endo, Y. Matsuo, and H. Ohta, ACS Appl. Mater. Interfaces **15**, 23512–23517 (2023).
[27]M. Yoshimura, Q. Yang, Z. Bian, and H. Ohta, ACS Appl. Electron. Mater. **5**, 4233–4239 (2023).
[28]K. Yamauchi and I. Hamada, Phys. Rev. B **108**, 045108 (2023).
[29]H. S. Choe, J. Li, W. Zheng, J. Lee, J. Suh, F. I. Allen, H. Liu, H.-J. Choi, W. Walukiewicz, H. Zheng, and J. Wu, Appl. Phys. Lett. **114**, 152101 (2019).
[30]J. J. Martin and G. S. Dixon, Phys. Status Solidi B **54**, 707–712 (1972).
[31]F. Serrano-Sánchez, J. L. Martínez, F. Fauth, and J. A. Alonso, Dalton Trans. **50**, 7085–7093 (2021).
[32]M. Namba, H. Takatsu, R. Mikita, Y. Sijia, K. Murayama, H.-B. Li, R. Terada, C. Tassel, H. Ubukata, M. Ochi, R. Saez-Puche, E. P. Latasa, N. Ishimatsu, D. Shiga, H. Kumigashira, K. Kinjo, S. Kitagawa, K. Ishida, T. Terashima, K. Fujita, T. Mashiko, K. Yanagisawa, K. Kimoto, and H. Kageyama, J. Am. Chem. Soc. **145**, 21807–21816 (2023).
[33]J. Cho, M. D. Losego, H. G. Zhang, H. Kim, J. Zuo, I. Petrov, D. G. Cahill, and P. V. Braun, Nat. Commun. **5**, 4035 (2014).
[34]S. Ning, S. C. Huberman, C. Zhang, Z. Zhang, G. Chen, and C. A. Ross, Phys. Rev. Appl. **8**, 054049 (2017).
[35]E. Langenberg, D. Saha, M. E. Holtz, J.-J. Wang, D. Bugallo, E. Ferreiro-Vila, H. Paik, I. Hanke, S. Ganschow, D. A. Muller, L.-Q. Chen, G. Catalan, N. Domingo, J. Malen, D. G. Schlom, and F. Rivadulla, Nano Lett. **19**, 7901–7907 (2019).
[36]B. M. Foley, M. Wallace, J. T. Gaskins, E. A. Paisley, R. L. Johnson-Wilke, J.-W. Kim, P. J. Ryan, S. Trolier-McKinstry, P. E. Hopkins, and J. F. Ihlefeld, ACS Appl. Mater. Interfaces **10**, 25493–25501 (2018).
[37]G. Wei, L. Wei, D. Wang, Y. Tian, Y. Chen, S. Yan, L. Mei, and J. Jiao, RSC Adv. **7**, 2644–2649 (2017).